METHOD ARTICLE

The Playground Shade Index: A New Design Metric for Measuring Shade and Seasonal Ultraviolet Protection Characteristics of Parks and Playgrounds

Nathan Downs[*1,2], Nawin Raj[2], Jennifer Vanos[3], Alfio V. Parisi[2], Harry Butler[1,2], Ravinesh Deo[2], Damien Igoe[2], Benjamin Dexter[2], Melanie Beckman-Downs[2], Joanna Turner[2], Stijn Dekeyser[2]

[1]. Centre for Applied Climate Science, University of Southern Queensland, Toowoomba, Australia, [2]. School of Mathematics, Physics and Computing, University of Southern Queensland, Toowoomba, Australia, [3]. School of Sustainability, Arizona State University, Tempe, AZ, USA.

[*] Corresponding author e-mail: nathan.downs@usq.edu.au (Dr Nathan Downs)

This article has been accepted for publication and undergone full peer review but has not been through the copyediting, typesetting, pagination and proofreading process which may lead to differences between this version and the Version of Record. Please cite this article as doi: 10.1111/php.13745

ABSTRACT

Current shading strategies used to protect outdoor playgrounds from harmful solar radiation include the placement of artificial cloth weaves or permanent roofing over a playground site, planting trees in proximity to playground equipment, and using vegetation or surface texture variations to cool playground surfaces. How and where an artificial shade structure is placed or a tree is planted to maximize the shade protection over specific playground areas, requires careful assessment of local seasonal sun exposure patterns. The Playground Shade Index (PSI) is introduced here as a design metric to enable shade and solar ultraviolet exposure patterns to be derived in an outdoor space using conventional aerial views of suburban park maps. The implementation of the PSI is demonstrated by incorporating a machine learning design tool to classify the position of trees from an aerial image, thus enabling the mapping of seasonal shade and ultraviolet exposure patterns within an existing 7180 m^2 parkland. This is achieved by modeling the relative position of the sun with respect to nearby buildings, shade structures, and the identified evergreen and deciduous tree species surrounding an outdoor playground.

INTRODUCTION

Outdoor playgrounds provide spaces for children to play, grow, learn and socially interact (1). These are often integrated within parklands, contributing to the availability of green space within an urban landscape, which in turn provide places for large trees, gardens and other natural features (2). These green spaces are often positively associated with improved health and well-being (3) and can facilitate social cohesion and resilience within urban society (4). The playgrounds embedded within parks vary across any given municipality depending upon the local geography, climate, land cover and the intended utility of that parkland. The types of parks encountered within a cityscape may include suburban pocket parks, open sporting fields, botanical gardens and nature preserves, large metropolitan recreational districts, neighborhood green spaces, or small local playgrounds (5). Good design can directly motivate adults to visit an area that will ultimately be used by accompanying children who visit a playground or make use of a park's available green space (6). Thus, a park may service an urban population by providing places for recreation, social gathering, or physical exercise and, if well-vegetated, contribute toward reducing the thermal load in developed environments (7,8,9).

Playgrounds within a parkland are environments exposed to the sun at all times of the year. They can therefore place visitors at risk of thermal stress and excessive sun exposure (10). Shading provided by trees, vegetation and physical shade structures is important (2,8,11), as behaviors when young (12) influence lifetime exposure patterns to solar ultraviolet (UV) radiation; that in turn contribute to the development of harmful skin and eye disease (13). The shade provided must therefore be fit for purpose and be capable of protecting users throughout

the day and also at relatively low sun angles. Such design strategies are important for shade structures located within tropical and sub-tropical climates where the solar UV can exceed high levels even in winter (14). Well-planted parks may provide ample protection from prolonged and harmful solar UV exposure; however, recent observations have revealed a prevalence of parks where the playground equipment is in direct sunlight (15,16,17). In many parks there is very little to no artificial or tree shade at all (17). Currently, there is no universal metric for assessing the solar UV protection in parks and playgrounds (8) and there is comparatively little research targeted at evaluating the existing shade level in parks, especially around playgrounds (8,15).

Shade audits are an important tool that can be used to assess the shade provision in a particular area. These audits often involve inspection of the location or interviews with the respective users of the park (18). A recent development in shade auditing has involved mapping tools, such as Google Earth and Google Street View (17). Important factors that need to be considered in assessing the shade and solar UV protection of a park include the assessment of the number of purpose-built shade structures, buildings and trees. Ideally, such assessments should also consider their position, size, shape and the corresponding sky view factor observed on site as this directly influences the shading pattern throughout the day and year (8,18,19). In designing a universally accepted metric to assess the spatial distribution of shade in favor of UV protection, a consistent methodology should be applied, allowing for fair comparisons to be made across the variety of different spaces that may be encountered within an outdoor park or playground for any time of day or year. Ideally, it should also facilitate accurate shade design specific to a given location. Such a tool can be valuable to designers in building new or

retrofitting playgrounds, as sun and heat protection are often overlooked, yet are important design aspects of such areas (20).

This research proposes a new methodology for deriving accurate shade and UV exposure surface patterns for a defined outdoor playground or park. A new metric, the Playground Shade Index (PSI) is introduced. The index expresses the ground site UV protection as an average for a specified outdoor region and defined time interval with respect to the available ambient UV. Its intended purpose is to aid shade designers when planning to develop or improve an existing outdoor park or playground. It is also introduced as a useful metric for making comparisons between existing parks, playgrounds and outdoor spaces to compliment and simplify existing shade auditing techniques. Its use is illustrated here by way of example for a single parkland occupying 7180 m^2 and situated in a suburban region of southern Queensland, Australia. The park includes a playground, a picnic shade structure, a range of established tree species, and surrounding buildings. Processes used to map the position of each parkland object are introduced, including the techniques used to model their solar UV protection characteristics.

MATERIALS AND METHODS

The PSI is presented and illustrated here by implementing a procedure that can be applied to existing aerial surface maps. The procedure is developed by firstly mapping the position of each surface object likely to shade an outdoor playground or park. These objects include trees, purpose-built shade structures, and nearby buildings. The relative surface shade pattern is

projected for each object onto the assessable parkland surface for a given period. Here, solar UV exposures are calculated as the approximated daily integral, evaluated in steps of five minutes from 5:00 am to 7:00 pm for each square meter of available parkland. The resulting surface solar UV exposure is expressed relative to the available ambient UV exposure for the same daily period and expressed as a parkland surface area average as the PSI.

The PSI is implemented and illustrated here using the Google Maps 2021 online representation of Paradise Park (27.61^{o}S, 151.94^{o}E), Toowoomba Queensland, Australia (Fig. 1a). The developed PSI is analogous to the Ultraviolet Protection Factor (UPF), a standard metric for assessing physical protection from biologically effective solar UVR (Equation 1) where the UPF is defined as the ratio of the available erythemogenic ambient solar ultraviolet irradiance, UV_{ery} (21) to the erythemogenic ultraviolet irradiance measured at a given site physically protected from incident solar radiation, UV_{site}.

$$UPF = \frac{UV_{ery}}{UV_{site}} \qquad (1)$$

The UPF has been employed previously for shade cloth sails (22), purpose-built shade structures (23,24), textiles (25), and sun-protective clothing (26). The UPF measured underneath standing shade structures in an open outdoor environment depends on the available UV_{ery} at the time of measurement and can vary depending on the position of the sun, the time of day and the season (23,27).

The PSI is used to assess the overall parkland protection from biologically effective solar UVR *in situ.* It is evaluated as the erythemogenic ultraviolet ambient exposure over a given period, *t=0* through *n*, expressed relative to the arithmetic mean of *r* square meters of parkland site exposures experienced over the same period within a defined playground space or area. Unlike the UPF, which defines the protection available at a single site, the PSI represents the average UPF for the entire defined playground or park region of *r* square meters (Equation 2).

$$SPI = \frac{\int_{t=0}^{n} UV_{ery}(t)\,dt}{\left[\sum_{site=1}^{r}\left(\int_{t=0}^{n} UV_{site}(t)\,dt\right)\right]/r} \qquad (2)$$

The PSI is designed to consider the UV exposure over a defined time period, *t = 0* to *n*. By making shade assessments with the PSI over an extended time period, the variability in shade protection with the sun's changing position can be accounted for so that different outdoor environments can be assessed and compared fairly over a standardized interval of time.

The Paradise Park Shade model: Paradise Park is located adjacent to the University of Southern Queensland, Toowoomba Campus. A model of each shading tree, shrub, shade structure and boundary object (fences, and building walls) was developed and is shown in plan view in Fig. 1b. The park covers a surface area of 7180 m^2. It is bordered on its northern and eastern sides by residential fence lines. Along some of these fence lines, there are low overhanging trees growing inside the residential properties that border Paradise Park. These low overhanging trees range in height from 2 to 4 m. On its western and southern sides, the park is lined by a row of 11 evergreen Hoop Pines (*Araucaria cunninghamii*, Fig. 1b, [b]). These trees reach heights of 7 to 10 m, and have a relatively narrow circular canopy diameter,

varying from 4 to 6 m. A total of four different deciduous species, *Jacaranda mimosifolia*, with generally larger canopy diameters ranging from 4 to 10 m, are located along the park's boundary at the northern end of West Street (Fig. 1b, [a]). Although wider in canopy diameter, these trees are lower in height than the park's Hoop Pines, reaching between 3 to 6 m. At the northern end of Paradise Park are six immature London Planetrees (*Platanus acerifolia*, Fig. 1b, [c]). *P. acerifolia* is a deciduous species, which has no foliage in the southern hemisphere park site from June through to August. In addition to the larger tree species, there are three centrally located shrubs (Fig. 1b, [d]) growing in the vicinity of an unprotected sand-based playground surface of 180 m^2 (Fig. 1b, [g]). These shrubs are a little over 2 m tall and each has a canopy diameter of approximately 3 m.

>FIGURE 1<

West of the park's sand-based playground area is a hexagonal roofed shade structure (Fig. 1b, [f]). The structure is large enough to seat six adults comfortably. The roof of the shade structure is steel and stands 2.3 m from the ground at its edges, rising to 3.5 m at the structure's center (Fig. 2). The structure is fenced on its northern and southern sides, from the ground to a height of 1.1 m and contributes to the structure's overall shade pattern.

>FIGURE 2<

Outside the south-eastern boundary of Paradise Park is a residential unit complex (Fig. 1b, [h]). The roof line and western wall of this residential complex adjoins the boundary of the

parkland and casts shade over Paradise Park in the early morning. All other surrounding buildings are located at least 2 m from the Paradise Park boundary and therefore do not cast shade onto the park during periods of high solar elevation. These surrounding buildings were not included in the Paradise Park shade model. In Fig. 1b, the park boundary is outlined in blue. The park includes the public footpaths adjoining West, Nelson, and Hennenlotter streets. Fence line boundaries are indicated in Fig. 1b in solid black outline at the park's northern, eastern and southern-eastern boundaries. The fence line includes part of the wall of the residential unit complex in the south-eastern corner of Paradise Park.

Modeling Tree Shade: *P. acerifolia*, *J. mimosifolia* and the three central shrubs surrounding the playground are modelled as tree species that include three distinct circular shading discs. The discs represent the canopy of each tree species. Each disc projects shade onto the park surface depending on the local solar elevation and azimuth. The park shrubs, *P. acerifolia* and *J. mimosifolia*, are classified here as having a rounded broom-canopy. The shading discs of these surface objects correspond with the approximate outline of an established tree (Fig. 3). For the broom-canopy shade model, the lowest shading disc of the tree is located horizontally at a quarter of the tree's total height (H). The second circular shade disc is of a smaller diameter than the lower disc, corresponding to the narrowing canopy, and is placed at 0.5 H. A smaller, third shade disc is placed at 0.75 H (Fig. 3b).

The total number of tree shade discs can be three, two, or one within the model, depending on whether a tree's shade is taken to represent the respective summer, autumn/spring, or winter season. For the deciduous tree species *J. mimosifolia* and *P. acerifolia*, only the smallest and

uppermost shade disc is utilized for the winter period June, July and August. The shade projected from the top-most disc is included in the winter period to take into account the potential shade that may still be cast onto the park surface by the tree trunk itself and its defoliated uppermost branches. The top two shade discs are utilized in our model to represent loose autumnal, or emerging springtime foliage for the mid-season months of May (autumn) and September (spring). All three shade discs are included for the months of October, November, December, January, February, March and April to accommodate the extended complete seasonal foliage density of *J. mimosifolia* and *P. acerifolia* in southern Queensland.

>FIGURE 3<

Figure 4 shows the corresponding seasonal shade pattern projected onto the surface of Paradise Park for *P. acerifolia* at 8:00 am local time on respective days in summer, autumn, winter and spring whereby this tree species experiences full foliage density on 04 January, full foliage density on 17 March, minimal foliage density on 13 July and partial foliage density on 20 September. The solar elevation angle for each figure frame representing the shade pattern at 8:00 am are 37^{o} (04 January), 27^{o} (17 March), 14^{o} (13 July), and 29^{o} (20 September). Reduced foliage in the winter shows that a reduced shade area is projected onto the parkland surface compared with the total shade area projected onto the park during summer and mid-season foliage periods. The lower solar elevation at 8:00 am in winter (Fig. 4c) also results in the projected shadow of the uppermost shade disc extending further westwards from the tree axis compared with the summer, autumn and spring 8:00 am shade projections of Fig. 4a, 4b and 4d respectively.

>FIGURE 4<

A similar three-disc shade model was used to represent evergreen tree species. The profile for evergreen *A. cunninghamii* is narrower at the canopy base than for deciduous species located in the park. To take into account the different canopy profile of *A. cunninghamii*, the lower canopy shade disc was located halfway along an evergreen tree's total height at 0.5 H. The second shade layer was placed at 2/3 H and the uppermost layer at 5/6 H. Thus, the width of successive canopy shade layers was reduced at a steeper rate, representing the increased narrowing of the canopy shown in Fig. 5.

>FIGURE 5<

Modeling Shade structures, buildings and fences: The remaining shade surfaces located within Paradise Park include the medium-sized shade structure, the neighboring boundary fences, and the nearby residential unit complex located on the park's south-eastern boundary. Each of these objects were modelled as solid geometric plane surfaces. They include individual roof sections, plane rectangular walls, and park boundary fence panels. Each of these shading surfaces was incorporated into the shade model by outlining the vertices of each solid surface section. The position of each surface section was referenced according to a 3-dimensional X, Y and Z Cartesian coordinate, measured from a fixed origin point (0,0,0) marked on the Paradise Park area map (Fig. 6).

All shading surface positions, including the center of all trees, and the solid parkland object shading surfaces, were located according to the park origin as indicated in Fig. 6. The origin was selected arbitrarily. In this case, the origin is marked by the position of a fixed signpost located in the bottom left of the park image. All tree positions and solid park shading surfaces were referenced relative to this position.

As well as their relative position, the heights of trees, buildings, shade structures and fences also influence the daily shade pattern projected onto the surface of Paradise Park. The heights of the park shade structure and three shrubs surrounding the park playground area were measured on site. The heights of large trees were derived by scaling the maximum shadow length measured from the center of each tree axis with respect to the known height of a single park shrub located a few meters west of the playground and south of the hexagonal shade structure (Fig. 6). The relative length of tree shadows scaled with reference to this tree determined that all *P. acerifolia*, *A. cunninghamii* and *J. mimosifolia* tree species ranged in height from 2 to 10 m.

>FIGURE 6<

Image classification by machine learning: The positions and canopy diameter of every tree can be obtained by direct measurement with respect to the park origin, as schematized in Fig. 6. However, because any given park may include many trees across a wide area, a machine learning (ML) image identification algorithm was also trialed, to support generic use outside controlled test sites. The outcomes of the algorithm were compared against the known position

and canopy diameter of each tree using the method discussed above. Tree locations inside Paradise Park were derived using a Java based image classifier (28). Fiji WEKA (Waikato Environment for Knowledge Analysis, (28)) allowed training and classification of image characteristics within an interactive online environment. The plan view of Paradise Park was examined using Fiji WEKA (28) to derive the diameter of individual canopies, and to classify the position of trees with respect to the park origin through the use of a Random Forest Classifier (RFC).

Random Forest Classifier (RFC): The RFC uses a combination of connected decision tree classifiers. Each classifier is generated using a random vector sampled independently from the input vector. Each RFC decision tree selects the most popular class to classify the input vector. Figure 7 shows the network architecture diagram of the ML decision trees of RFC, where x is the input vector for each individual image pixel and k_i is the decision output. The architecture is based on the principle of randomized ensembles of decision tree nodes (29). Each binary decision tree is constructed using a recursive partitioning sequence. Every decision tree votes in this process and the most popular class is selected as the result. Binary splits ensure homogeneity or near homogeneity with splitting into daughter nodes from a parent decision tree (30).

>FIGURE 7<

The ML algorithm generates a forest of classification decision trees (RFC) based on the bootstrapping of image feature data and assigned classes chosen from user defined pixel

regions. Defined pixel regions included samples of pixels from Fig. 1a belonging to *A. cunninghamii*, *J. mimosifolia*, and *P. acerifolia*. After the model classifier was developed, it was used to segment the input image to classifier image features. The ML algorithm used numerous classification decision trees to 'vote' for which class an image pixel would be assigned with respect to its features and built decision trees from the dataset by bootstrapping. Class bins defined by the Fiji WEKA (28) algorithm included the 'Hessian', 'Membrane projections', 'Difference of Gaussians' and 'Homogenize classes' check options. Fiji WEKA (28) image segmentation settings were set at a membrane thickness of 1, a membrane patch size of 19, minimum sigma of 1.0, and maximum sigma of 16.0. Figure 8 shows the resulting classification of the trained model.

>FIGURE 8<

The difference of Gaussians setting applied using Fiji WEKA (28) calculated two Gaussian blur images from the original image and subtracted one from the other. The Gaussian blur performs four convolutions with Gaussian kernels ($\delta = 1, 2, 4 \text{ and } 8$). After the Gaussian blur was applied, the Sobel operator, or filter, calculated the gradient at each pixel. The Hessian setting of the Fiji WEKA (28) application calculated the Hessian matrix at each pixel as:

$$H(f) = \begin{bmatrix} \frac{\partial^2 f}{\partial x^2} & \frac{\partial^2 f}{\partial x \partial y} \\ \frac{\partial^2 f}{\partial x \partial y} & \frac{\partial^2 f}{\partial y^2} \end{bmatrix}. \qquad (3)$$

The Hessian matrix has the following properties:

1. $\frac{\partial^2 f}{\partial x^2}$ – the *x*-direction Sobel kernel is convolved with the image twice;
2. $\frac{\partial^2 f}{\partial y^2}$ – the *y*-direction Sobel kernel is convolved with the image twice; and
3. $\frac{\partial^2 f}{\partial x \partial y}$ – the *x* and *y* direction Sobel kernels are each convolved with the image once.

Machine Learning defined Tree Species Parameters: Once the tree canopy positions were separated from the background of Fig. 8, the result was further processed to calculate the local Cartesian coordinates of each individual tree and their respective canopy diameters. This was done by taking the 8-bit image of Fig. 8 and applying the Fiji WEKA (28) watershed tool to develop clearly defined boundaries for each set of classified image pixels, shown in Fig. 9.

>FIGURE 9<

The regions defined in the processed image as trees were numbered using the analyze particles function of Fiji WEKA (28) to identify and associate the measured canopy values of each tree (Fig. 10). Table 1 shows a sample of the measured tree species canopy parameters derived from the ML algorithm. The local (*x*, *y*) image coordinate reference point of Fig. 10 was taken as the upper left-hand corner of the processed image (0,0), where the values, measured in pixels increase positively to the right (*x*-direction) and downward (*y*-direction). Local image coordinates identified by the algorithm of the processed image were later transcribed by vector

subtraction to derive the individual position vectors of each tree expressed relative to the local shade map origin and scaled to the size of the analyzed image (Fig. 6).

>TABLE 1<

>FIGURE 10<

The diameter of each tree canopy is approximated in Table 1 assuming a circular canopy foliage area. Table 2 compares the approximate canopy diameter derived by the ML algorithm for each sample tree listed in Table 1 to the approximate canopy diameter measured by the Google map measurement tool. Both estimates of canopy diameters show reasonable agreement, indicating that the manual use of the Google maps measurement tool can be safely replaced.

>TABLE 2<

The X, Y position of all tree trunks and all tree canopy diameters depicted in the park surface objects modeled in Fig. 1b were derived from measurements in Google maps. By modeling each surface object and their relative position within the boundaries of Paradise Park, the shade, solar UV exposure, and PSI were able to be determined for the whole 7180 m^2 park surface. In this research, the PSI was derived over a daily interval for each of the summer, autumn, winter and spring seasons from 5:00 am to 7:00 pm.

RESULTS

Local ambient ultraviolet exposure: In the calculation of PSI, the UV irradiance, UV_{ery} was calculated by summing the diffuse erythemogenic solar ultraviolet irradiance, UV_{diff} and the direct shadow causing erythemogenic ultraviolet irradiance, $UV_{dir.}$ The direct and diffuse solar UV components can be measured if local instrumentation is available, or alternatively predicted using a model. For this research, UV_{ery} was determined over a daily interval from 5:00 am to 7:00 pm for cloud-free skies. Here, the direct and diffuse UV irradiance components were derived according to Rundel's (31) modification to the original semi-empirical calculations of Green, Sawada and Shettle (32), Green, Cross and Smith (33) and Shippnick and Green (34). These equations derive the local direct and diffuse UV irradiance based upon approximations to the radiative transfer calculations of Braslau and Davé (35,36,37) and Dave and Halpern (38). The application of these calculations for the direct and diffuse UV irradiance utilize local solar elevation, aerosol optical depth (AOD), and total column ozone (TCO) as inputs from which the calculated surface spectral irradiance can be weighted to the human erythema action spectrum (21).

The ambient model output is a daily time series of the cloud-free irradiance, UV_{ery}. UV_{ery} was derived for Paradise Park in 10-minute intervals from 5:00 am to 7:00 pm, Australian Eastern Standard Time (AEST) for single days of the summer, autumn, winter and spring seasons depending on the daily local solar position in azimuth and altitude at each time step. The solar position was calculated according to Michalsky's (39) algorithm for local solar position at the southern latitude of Paradise Park. The modeled UV_{ery} closely approximates local measurements of the spectrally weighted UV irradiance taken under cloud-free conditions.

Figure 11 compares Rundel's (31) approximation of the local UV_{ery} calculated in 10-minute steps from 5:00 am to 7:00 pm for atmospheric input parameters including an AOD of 0.4 and TCO of 370 DU, 410 DU, 440 DU and 460 DU for the cloud-free dates of 04 January 2014 (summer), 17 March 2013 (autumn), 13 July 2013 (winter), and 20 September 2013 (spring) to the locally measured spectral UV irradiance made simultaneously using a Bentham DTM300 double monochromator (Bentham Instruments, Reading UK). Cloud-free model irradiance parameters were chosen arbitrarily to approximate the measured UV_{ery} daily profile recorded by the Bentham DTM300 in each season. Ambient Bentham DTM300 double monochromator UV irradiance scans are weighted to the human erythema action spectrum and recorded over a range of 280 to 400 nm at a 0.5 nm wavelength resolution. This instrument is located on an open rooftop site at the University of Southern Queensland, situated less than 900 m from Paradise Park. Measurements shown in Fig. 11 were taken over 10-minute intervals with results traceable to the National Physical Laboratory UK standard. Instrument irradiance measurements have a quoted uncertainly of ±9% (40).

Figure 11 shows the modeled peak solar noon ambient UV_{ery}. The irradiance values may also be expressed in terms of the UV index (41), where 1 is the equivalent of 25 mW m^{-2} erythemogenic UV. Figure 11 indicates the seasonal noon-time peak variation in daily UV index at Paradise Park varies from approximately 11 (275 mW m^{-2}) in summer to 2.5 (60 mW m^{-2}) in winter under cloud-free conditions. The figure also shows the influence of seasonal solar elevation with local time for Toowoomba's 27.5ºS latitude, with the peak noon irradiance shifting from approximately 12:00 pm in winter to 12:30 pm in summer. The daily ambient erythemogenic exposures, calculated as the integral of the UV_{ery} over the 14-hour

interval from 5:00 am to 7:00 pm for each of the respective summer, autumn, winter and spring days (Fig. 11) are 58.8 SED, 34.6 SED, 11.0 SED and 27.8 SED, where 1 SED is the equivalent of 100 J m^{-2} (42). These modeled daily exposures represent the ambient UV_{ery} integral from *t=0* (5:00 am) to *n* (7:00 pm) in Equation 2 and were used as the ambient exposures for defining the seasonal PSI of Paradise Park.

>FIGURE 11<

Park site ultraviolet exposures: The modeled erythemogenic direct and diffuse solar ultraviolet irradiance components were weighted to the local park surroundings to derive UV_{site} for each square meter in the 7180 m^2 park. Here, the integrated erythema UV irradiance at a single park site is derived by applying Equation 4 for each square meter, *p* depending on the approximated local sky view and the probability that the sun is directly blocked by local surroundings, P_0 over the defined exposure period, *t=0* to *n*.

$$\int_{t=0}^{n} UV_{site}\,(t) = \int_{t=0}^{n} \left((1 - OS).UV_{diff}(t) + P_0.UV_{dir}(t)\right) dt \qquad (4)$$

Site Sky fraction: To determine the total available sky fraction, the fraction of sky obscured by surface objects, *OS* at any given park location, *p* was first calculated according to the approximate relative cover available at that site (Fig. 12). *OS* is independent of the time of day as it represents the fixed fraction of sky that is likely to be obscured at a given park site by static park surface objects such as trees and surrounding shade structures. In the example shown in Fig. 12, *OS(x,y)* depends on the obstruction of surrounding trees and overhead shade

structures located in each surrounding square meter, *p(x-1,y-1)* to *p(x+1,y+1)* on a 3×3 grid where for each square meter, $p = 1$ represents an obstructed shade state, and $p = 0$ represents an open sky shade state. The local *OS(x,y)* in this example is calculated as 0.1 multiplied by the sum of all nine shade states in each of the surrounding square meters and the site itself, *p(x,y)*. Using this methodology, park sites completely obscured over all eight surrounding square meters and the site *p(x,y)* would have an *OS* = 0.9. The effective sky view at that site is then calculated by the factor *(1 – OS)* in Equation 4. This assumes that a completely obscured park site allows at least 10% of the available sky to be observed. Conversely, for open park locations with no surrounding cover, the obstructed sky fraction, *OS* would be 0, resulting in 100% of the available diffuse solar UV contributing to UV_{site} in Equation 4. The equation assumes an isotropic diffuse UV skylight distribution weighted directly to the available sky fraction at a given park surface site. This assumption is reasonable for a short wavelength erythemogenic UV spectrum which exhibits less dependence on the whole sky radiance distribution than, for example, longer UVA or visible solar radiation total sky distributions, which tend to experience higher diffuse radiance distributions toward the horizon (43).

>FIGURE 12<

To determine if a given park site sky view was likely to be protected by a tree or a surrounding shade structure, each square meter of Fig. 1b was compared to the position of each parkland surface object. In this case, the diameter of individual tree lower shade discs, and the area of each roof panel of the hexagonal shade structure was used to determine which parkland sites, *p* would be obscured by a surface object. Calculation of site sky view factors (1-*OS*) were

limited to all parkland square meter sites located within 1 m of the defined boundary of Paradise Park, thus accommodating the 3×3 grid used to calculate local site *OS*.

Site sun obstruction: The direct UV irradiance contribution to a given parkland exposure site is dependent on the position of the sun and the relative position of surface objects mapped within the park. This is accounted for in Equation 4 by the inclusion of a sun obstruction probability factor, P_0. Here, $P_0 = 1$ if the sun is unobstructed by a park surface object such as a tree canopy or shade structure, and $P_0 = 0$ if the sun is blocked. To determine if the sun is obscured or not over the daily exposure interval $t=0$ through n, the shade distribution for each surface object was projected onto the horizontal park surface at each 10-minute interval in the day from 5:00 am to 7:00 pm.

Using simple geometric surfaces to represent tree canopies, shade structures and fences, the projected shade pattern of each parkland surface object was able to be determined from Michalsky's (39) solar position model, using the known position and height of every parkland surface object. As an example, a point located on the edge of the hexagonal shade structure's roof line that is at a height, h will cast to a known shadow distance onto the park surface, S_d. For example, at 9:30 am on 13 July S_d will be 4.1 m from the position of the shade structure's 2.3 m high roof line. The shadow will be cast along a path that is 40^o west of south (southern hemisphere), given the local azimuth at that time will be 40^o, and the local solar zenith angle (SZA) will be 61^o. In the example, the length of the shadow of 4.1 m is calculated using Equation 5.

$$S_d(t) = h \tan(SZA(t)) \quad (5)$$

By tracing the projected position of points located on the edges of tree canopies, fences and shade structure surfaces onto the horizontal park surface, the shade state, P_0 of each square meter of Paradise Park can be determined for any date and time.

Park shade projections: Figure 13 illustrates the modeled shade projection for the park's hexagonal shade structure on 20 July 2021 from 4:00 pm to 4:10 pm. The figure compares the modeled shade projection with an image photographed in the park at 4:10 pm on the same day with the sun in the west (301^o) and at low solar elevation (12^o). In the photograph, the shade from the hexagonal shade structure, including all roof and shade structure fence surfaces, is seen projected onto the western edge of the sand surfaced playground. The shade pattern corresponds with the modeled shade position at the same time of day. Short-term shade patterns projected from each tree, building, shade structure and fence line are illustrated in Fig. 14. In Fig. 14, park shade patterns are compared to a drone image facing south-east imaged from the park's north-western boundary on 16 November 2021 at 9:50 am (76^o solar azimuth, 64^o solar elevation). The comparison shows that the use of simple geometric shading surfaces used to represent parkland trees and shading surfaces can produce projections that closely match photographed shade patterns experienced at the same time date and time.

>FIGURE 13<

>FIGURE 14<

The overall likelihood that a given park site will be protected by shade can be calculated from the daily projected shade pattern corresponding to the solar elevation and azimuth in each of the 84 ten-minute time intervals between 5:00 am to 7:00 pm. In this research, the likelihood that a given parkland site is protected by shade is expressed as the surface shade level where a shade level of 100% represents a surface site protected by shade during each of 84 ten-minute daily intervals in the period 5:00 am to 7:00 pm. Thus, shade level represents the proportion of time each square meter of parkland is protected by shade.

Park shade level for the 5:00 am to 7:00 pm daily interval of 04 January, 17 March, 13 July and 20 September is presented in Figs. 15a, 16a, 17a and 18a respectively. Immediately evident in the Paradise Park shade level is the seasonal influence of the changing solar declination angle. In January, the sun is two weeks past its maximum southern celestial declination, occurring on 21 December on the solstice. As a result, the sun rises on 04 January in the south-east and reaches to within 4^{o} of the local zenith before setting in the south-west. The resulting shade pattern reflects the seasonal southern declination of the sun as shown by Fig. 15a shade projections in the early morning to the north-west, and north-easterly shade projections in the late afternoon. At this time of year, *P. acerifolia* and *J. mimosifolia* experience their highest foliage density. However, shade patterns in Fig. 15a are not projected far from the trees and other parkland surface objects during the course of a day.

Tree foliage density is also high in the shade level map shown in Fig. 16a. However, as the solar celestial declination angle at this time of year approaches 0^{o}, the sun rises almost directly in the east and sets in the west. The resulting shade pattern, while projecting a little further

south, as the sun traverses a northerly path, runs approximately in a linear east-west direction. A direct east to west shade pattern is also evident in Fig. 18a for 20 September, with the sun being very close 0^o declination at the equinox, however the reduced foliage density of *P. acerifolia* and *J. mimosifolia* in September results in a little less shade being projected onto the surface of Paradise Park in proximity to the two deciduous tree species located at the northern end of the park. The highest shade level is observed in winter (13 July). On this date, the sun's northern declination angle results in the sun traversing a much lower trajectory than observed in September or March, reaching a maximum daily elevation of 39^o. Again, because of the sun's northern declination in winter, early morning shade patterns are projected to the south-west, as the sun rises in the north-east, and are projected to the south-east as the sun sets in the north-west. During the winter, although *P. acerifolia* and *J. mimosifolia* have minimal foliage, a generally higher park shade level is observed in proximity to the park's trees and shade structure.

PSI and daily UV exposure: Having calculated the probability, P_0 that a given park site will be protected by shade, and the local sky fraction for each square meter of available parkland, Equation 4 was used to derive UV_{site} for the entire surface area of Paradise Park. Over each 10-minute interval between $t = 0$ at 5:00 am *and* $t = n$ at 7:00 pm, the UV_{site} irradiance was multiplied by 600 seconds to derive the daily UV exposure received for each square meter of the parkland. The erythemogenic solar exposure for 04 January, 17 March, 13 July and 20 September is plotted in Figs. 15b, 16b, 17b and 18b, respectively. These figures are also repeated in Figs. 15c, 16c, 17c and 18c without plotting individual surface objects showing the

expected UV exposure pattern directly beneath each tree and the park's hexagonal shade structure.

>FIGURE 15<

>FIGURE 16<

>FIGURE 17<

>FIGURE 18<

The maximum and parkland average daily erythemogenic exposure for Figs. 15, 16, 17 and 18 are listed in Table 3. Using the calculated ambient and average park site UV exposure, the PSI was derived for the period 5:00 am to 7:00 pm for the cloud-free conditions experienced over Paradise Park on 04 January 2014, 17 March 2013, 13 July 2013, and 20 September 2013. The PSI derived for these four days shows little variation between the seasons. For Paradise Park, the PSI varies between 1.09 and 1.08, falling only to 1.08 in winter when *P. acerifolia* and *J. mimosifolia* experience their minimal seasonal foliage density. As demonstrated here, the metric is not sensitive to the sun's position, given the daily ambient exposure and park average is calculated for an entire day. Rather, the PSI is influenced directly by the available sky view factor in each square meter of parkland and the daily shade level. These physical playground properties are influenced by the size and position of individual trees and shade surfaces situated within the park.

>TABLE 3<

DISCUSSION

The use of outdoor parks and playgrounds by both children and adults are an essential component for wellbeing, exercise, learning and play. Associated with all of these outdoor spaces are UV radiation exposures. The magnitude of these exposures is influenced by a number of factors, including the amount of shade determined by the number and quality of trees, surface vegetation and the presence of physical shade structures, as well as the time of the day and season. The quantification of the UV protection provided by stand-alone shade structures (27,44) and by individual trees (45) has been reported previously. Shade assessments of outdoor play areas, including parks are also common with many of these studies indicating limited protection in outdoor areas frequently used by parkgoers (15,46,47,48). The introduction of the PSI, developed in this research, has been designed to complement previous studies of solar UV protection and playground shade assessments by introducing a metric that incorporates every tree and surrounding surface structure that may shade the area defined by a user specified boundary.

The calculation of shade quality by each tree and roofing surface in Paradise Park was simplified in the current assessment by assuming complete opacity to direct ultraviolet radiation, UV_{dir}. Although the seasonal quality of shade was examined by modifying the number of tree canopy discs, the opacity of each shading disc within a tree canopy is also likely to change with season and between tree species. This can be accounted for by modification of Equation 4 and the probability that direct solar UV will be blocked by a surface object, P_o. Future studies specifically designed to examine the influence of different shading materials or canopy density could utilize measured variations to the factor, P_o. For

example, in Equation 4, instead of P_o being 1 (transparent) or 0 (opaque), the factor could be changed to 0.5 for materials known to block 50% of the available UV_{dir}, or 0.25 for materials known to block 75% of the available UV_{dir}. Measurement of different roofing materials and of different canopy foliage density between tree species utilized in parks and playgrounds will add to future assessments made using the PSI.

The PSI introduced here is intended to provide a new and valid metric for making fair comparisons of shade and solar ultraviolet protection over large outdoor spaces. It has the potential to be used across a range of different park and playground types to enable future comparisons with and across different urban environments and municipalities. In calculating the PSI, the local height and size of each shading object situated within the defined park or playground area is considered. The demonstrated technique allows quantification of the UV protection provided by the combined influence of modeled tree canopies and artificial shade structures for the different solar elevations and azimuths encountered throughout any given day of the year. In this research, the PSI was derived for cloud-free days occurring in the summer, autumn, winter and spring. Each measured PSI demonstrates that the UV exposure, when expressed as a parkland average of the available ambient varies by only 1.08 to 1.09, indicating, in this application that the PSI metric is a good measure of the protective characteristics of the park, and is not necessarily dependent on the available ambient. There may still remain however, the need for consideration of seasonal solar variations that are experienced at a park or playground, as the available ambient UV exposure on any given day will vary with the diurnal position of the sun. The PSI taken for example at an interval near midday will likely be different to the PSI measured in the later afternoon or evening. When

these variations are taken into account, the introduced PSI may be used as a standard to make comparisons between different parks and playground spaces that experience the same ambient UV exposure for any consistent interval of time.

Here, the range in observed PSI is small to negligible between the seasons. The overall size of the park, and the limited number of trees and shading surfaces in the park's center are likely to have contributed to the low overall protection of the park as a whole. PSI comparisons made between different parks that utilize an average parkland UV exposure are therefore subject to variations that are dependent upon their total size and the relative density of shading objects within the defined parkland borders. How and where the defined PSI border is defined depends largely upon a user's assessment methodology and aim. Projects designed specifically to investigate the shade and UV protection of the playground surface may define a boundary limited only to that surface. Researchers wanting to investigate different zones within a large park may similarly divide their PSI boundaries accordingly.

This research has taken advantage of publicly accessible aerial views of a parkland. While not all regions of the earth have been surveyed in detail (49), the availability of such data that can be accessed online, highlights the value of surveys that can be conducted remotely. The functionalities of traditional mapping tools and auditing techniques (50,51) and even those that make use of Google Street View including, for example, those recently implemented by Gage et al. (17) can be further improved by using our proposed technique to accurately map the spatial position of shade and UV exposure in existing landscaped park or playground regions. The PSI, including the use of ML for identification of parkland surface objects is therefore a

potentially powerful new shade and environmental UV auditing tool that can be used to assess outdoor spaces not readily accessible to field researchers.

Machine learning: Publicly accessible imagery has recently been highlighted as a promising tool for automated environmental assessment for health research, including park design (49). The present research provides the prospect of building a robust ML-based classification method that can be used for auditing shade requirements in parks and playgrounds. This study has demonstrated the feasibility of ML, through the use of a readily accessible image classifier (28) to improve and complement existing computer software already provided by aerial maps sourced using Google Earth for the measurement of spatial park and playground characteristics. The ML algorithm is introduced here to demonstrate the image training potential of readily available online toolsets. An approach that uses ML to find, identify and correctly position parkland trees, shade structures, and buildings can save a significant amount of time for any shade designer intending to audit a large outdoor space, or a number of different outdoor parks using the PSI. It is not however, a compulsory requirement to use ML to develop the parkland PSI.

By implementing an ML approach to parkland surface object identification, the relative position and canopy diameters of all trees were able to be confirmed in the current case, quickly and with high precision. This research implemented a Random Forest Classifier (RFC) to identify and successfully locate the position of all trees within Paradise Park. Image processing techniques such as RFC have been shown in previous research to be very effective at identification of image features. The RFC method shows superior ability with its non-

parametric nature, high classification, and capability to determine the importance of image variables (52,53,54). However, alterative ML classification techniques may show improved results, particularly in different settings and could therefore be applied for future surface object classification across a range of parks, playgrounds or outdoor spaces.

Irrespective of the surface object classification technique used, the PSI, implemented through a ML approach can greatly increase the speed of identifying individual tree locations in a parkland or outdoor space. ML automation can enable faster surface object identification with our approach allowing the position of surface objects and therefore, the PSI to be calculated over large or multiple outdoor areas. This may otherwise be a tedious task if practiced manually for each individual tree or parkland object. The use of ML, implemented in this case using Fiji WEKA (28) has the potential to accurately identify surface objects in parks that may incorporate a high tree density. However, this has yet to be tested. Therefore, large scale, comparative assessments of parks using ML to identify surface objects that shade a defined outdoor space is an avenue for further research that requires testing over a range of aerial images, including different tree species, and surfaces with different ground covers such as asphalt, sand, concrete and grass. Such wide scale audits that implement ML should also be tested over a range of climatic and seasonal conditions including testing of aerial images taken in dry and wet seasons, testing of images that include variations in autumnal canopy foliage and testing of images that include surfaces covered with snow.

Limitations: This research has investigated the range in PSI for a single parkland environment located in southern regional Queensland, Australia. While only a single park, Paradise Park

has been used as an outdoor field site to assess the solar ultraviolet protection offered by purpose-built shade structures in past research (23,27,44). This past work has concluded that the solar protection offered by parkland structures is seasonally dependent. These findings could again be investigated using the PSI, a metric that has been developed independently of the need to take UV_{ery} measurements on site. As a design tool, the PSI therefore has the potential to measure the shade and ultraviolet protection of any newly planned shade structure, playground shade sail or intended tree plantings. This application of the PSI and the variations that may occur over different exposure periods will be investigated in future research.

While shade audits and UV protection surveys have been conducted previously in a range of parks, playgrounds and environments, the technique developed in this research has demonstrated how the use of shade structures and trees can protect surfaces over a broad spatial area. This can be advantageous over studies that survey UV protection at a chosen parkland site, such as the center of shade structures, or at predefined points in a playground, because mapping the shade and UV exposure over a defined surface area gives an indication of the individual contribution parkland surface objects make to the protection of the whole space that is potentially accessible to users. This has benefits for auditing of existing parks, playgrounds and outdoor spaces, but also for future design. One limitation however in the current parkland assessment using the PSI is that the location of shade is not taken into account with respect to dedicated play equipment. So, even though the perimeter of the park may be well protected year-round by *A. cunninghamii* and *J. mimosifolia* tree species, the seasonal PSI does not specifically weight parkland zones with respect to potential use. Here, the defined space used in calculating the PSI needs to be carefully managed depending on the

application. The PSI could for example, be modelled only within the confines of the parkland's sand surface playground, park benches, or its shade structure. The example given in this research has focused on the whole 7180 m^2 park.

The PSI implemented here was derived as the ratio of the available ambient UV exposure from 5:00 am to 7:00 pm and expressed as a park average. Evaluations were conducted assuming a cloud-free atmosphere over selected summer, autumn, winter and spring days. For most cases, a cloud-free atmosphere will result in a higher relative ambient UV exposure than for a sky partially or totally obstructed by cloud. In some cases, broken cumulus cloud cover, can elevate the ambient UV above that experienced under a cloud-free sky (55). These cases might be taken into account through improvements to the ambient UV exposure model. Cloud modification factors have previously been published and are available, which attenuate the expected UV exposure (56). The UV irradiance model of Rundel (31) implemented in this research may for example be paired with the cloud modification factor of Josefsson (57) where the modified UV irradiance, UV_{cloud} is dependent upon the total sky cloud fraction c,

$$UV_{cloud} = UV_{ery}(1 - 0.7c^{2.5}). \quad (6)$$

Although such models can be applied under cloud affected atmospheres, their application for the calculation of the PSI are likely to introduce uncertainties due to clear differences experienced in the whole sky UV radiance distribution when diffuse UV radiation may be absorbed or scattered by the presence of cloud of different type, altitude and position. Any site partially obscured by a parkland surface object will need to take into account the modified

radiance of UV_{diff} included in Equation 4 and the individual position of clouds with respect to each surface site. This again is an avenue for further research. Here, the purpose of the PSI is to provide a metric for quantitative assessment of solar UV and shade protection offered by surface objects in playgrounds and parks. This can be achieved through surface solar exposure assessments made using a cloud-free atmosphere.

The PSI may be beneficial in guiding skin and eye health promotion programs, particularly reducing skin cancer and eye disease through better urban planning, design, sun exposure policy development, and local government infrastructure provision relating to approvals for new residential or industrial development areas. To improve landscape design strategies for urban populations, the impact of the ultraviolet protection factor provided by urban trees in particular needs to be better understood (58). The introduced methodology demonstrates the potential of the PSI to make global shade assessments of parks, playgrounds, schoolyards and outdoor public spaces through the consideration of the total UV exposure received for a defined period of time. Here, the protection provided by surface objects located in a park was examined over a daily exposure period. Depending on the application, the PSI may be used to make fair assessments of the shade and ultraviolet protection provided for any specified interval of time. It can be used to fairly compare different parks, playgrounds and outdoor spaces, and it introduces a metric that can be easily understood to better define the characteristics that directly contribute to improved solar protection in outdoor environments.

ACKNOWLEDGEMENTS*:* Nathan Downs received financial support under the University of Southern Queensland Academic Development and Outside Studies Program 2022, which aided the completion of this research.

SUPPORTING INFORMATION

Additional supporting information may be found online in the Supporting Information section at the end of the article:

Section S1. Using the Playground Shade Index

REFERENCES

1. Gil-Madrona, P., M. Martinez-Lopez, A. Prieto-Ayuso, L. Saraiva, J. Vecina-Cifuentes, T. Vincente-Ballesteros, R. Moratilla-Lopez and G. Lopez-Sanchez (2019) Contribution of public playgrounds to motor, social, and creative development and obesity reduction in children, Sustainability, 11:3787, doi.org/10.3390/su11143787.

2. Taylor, L. and D.F. Hochuli (2017) Defining greenspace: multiple uses across multiple disciplines, Landscape Urban Plan. 158, 25-38.

3. Douglas, O., M. Lennon and M. Scott (2017) Green space benefits for health and well-being: a life-course approach for urban planning design and management, Cities, 66, 53-62.

4. Campbell, L.K., E.S. Svendsen, N.F. Sonti and M.L. Johnson (2016) A social assessment of urban parkland: Analyzing park use and meaning to inform management and resilience planning, Environ. Sci. Policy. 62, 34-44.

5. Ibes, D.C. (2015) A multi-dimensional classification and equity analysis of an urban park system: a novel methodology and case study application, Landscape Urban Plan. 137, 122-137.

6. Refshauge, A.D., U.K. Stigsdottir and N.G. Cosco, 2012, Adults' motivation for bringing their children to park playgrounds, Urban For. Urban Gree. 11, 396-405.

7. Deng, J., B.J. Pickles, S.T. Smith and L. Shao (2020) Infrared radiative performance of urban trees: spatial distributions and interspecific comparison between ten species in the UK by in-situ spectroscopy, Build. Environ. 172:106682.

8. Holman, D.H., G.T. Kapelos, M. Shoemaker and M. Watson (2018) Shade as an environmental design tool for skin cancer protection, Am. J. Public Health. 108, 1607-1612.

9. Astell-Burt, T., X. Feng and G.S. Kolt (2014) Neighborhood green space and the odds of having skin cancer: multilevel evidence of survey data from 267072 Australians, J. Epidemiol. Commun. Health. 68, 370.

10. Kennedy, E., H. Olsen, J. Vanos, D.J. Vecellio, M. Desat, K. Ruchters, A. Rutledge and G.R.A. Richardson (2021) Reimagining spaces where children play: developing guidance for thermally comfortable playgrounds in Canada, Can. J. Public Health. 112, 706-713.

11. Diffey,B.L. (2003) Human exposure to solar ultraviolet radiation, J. Cosmet. Dermatol. 1, 124-130.

12. Wright, C.Y. and A.I. Reeder (2007) Youth solar ultraviolet radiation exposure, concurrent activities and sun-protective practices: a review, Photochem. Photobiol. 81, 1331-1342.

13. Lucas, R.M. S. Yazar, A.R. Young, M. Norval, F.R. de Gruijl, Y. Takizawa, L.E. Rhodes, C.A. Sinclair and R.E. Neale (2019) Human health in relation to exposure to solar ultraviolet radiation under changing stratospheric ozone and climate, Photochem. Photobiol. Sci. 18, 641-680.

14. Turnbull,D.J. and A.V. Parisi (2006) Effective shade structures, Med. J. Aus. 184, 13-15.

15. Schneider, S., A. Bolbos, P. Kadel and B. Holzworth (2020) Exposed children, protected parents; shade in playground as a previously unstudied intervention field of cancer prevention, Int. J. Environ. Health Res. 30, 26-37.

16. Olsen, H., E. Kennedy, J.K. Vanos (2019) Shade provision in public playgrounds for thermal safety and sun protection: a case study across 100 play spaces in the United States, Landscape Urban Plan. 189, 200-211.

17. Gage, R., N. Wilson, L. Signal, M. Barr, C. Mackay, A. Reeder and G. Thomson (2018) Using Google Earth to assess shade for sun protection in urban recreation spaces: methods and results, J. Commun. Health. 43, 1061-1068.

18. Parisi, A.V. and D.J. Turnbull (2014) Shade provision for UV minimization: a review. Photochem. Photobiol. 90,479-490.

19. Li, X., C. Ratti and I. Seiferling (2018) Quantifying the shade provision of street trees in urban landscape: a case study in Boston, USA, using Google Street View, Landscape Urban Plan. 169, 81–91.

20. Kennedy, E., H. Olsen, D.J. Vecellio and J.K. Vanos (2020) Thermally comfortable playgrounds: a review of literature and survey experts, Technical Report, Health Canada and Standards Council of Canada.

21. Commission Internationale de l'Eclairage (CIE), Erythema Reference Action Spectrum and Standard Erythema Dose, ISO 17166:1999 (CIE S 007/E:1998), 1998.

22. Gies, P., J. Makin, S. Dobbinson, J. Jarvorniczky, S. Henderson, R. Guilfoyle and J. Lock (2013) Shade provision for Toddlers at swimming pools in Melbourne, Photochem. Photobiol. 89, 968-973.

23. Turnbull, D.J., A.V. Parisi and J. Sabburg (2003) Scattered UV beneath public shade structures during winter, Photochem. Photobiol. 78, 180-183.

24. Gies,P. and C. Mackay (2004) Measurements of the solar UVR protection provided by shade structures in New Zealand primary schools, Photochem. Photobiol. 80, 334-339.

25. Gambichler, T., K.L. Hatch, A. Avermaete, A. Bader, M. Herde, P. Altmeyer and K. Hoffmann (2002) Ultraviolet protection factor of fabrics: comparison of laboratory and field-based measurements, Photodermatol. Photoimmunol. Photomed. 18, 135-140.

26. Ranjan Das, B. (2010) UV radiation protective clothing, Open Tex. J. 3, 14-21.

27. Parisi, A.V., A. Amar, N.J. Downs, D.P. Igoe, S.L. Harrison and J. Turner (2019) Development of a model for calculating the solar ultraviolet protection factor of small to medium sized shade structures, Build. Environ. 147, 415-421.

28. Fiji WEKA 2021 Trainable Weka Segmentation, Available at: https://imagej.net/plugins/tws/. Accessed on 11 July 2022.

29. Breiman, L. (2001) Random forests. Mach. Learn. 45, 5-32.

30. Nguyen, C., Y. Wang and H.N. Nguyen, 2013. Random forest classifier combined with feature selection for breast cancer diagnosis and prognostic, J. Biomed. Sci. Eng. 6:31887.

31. Rundel, R. (1986) Computation of spectral distribution and intensity of solar UVB radiation. In Stratospheric Ozone Reduction, Solar Ultraviolet Radiation and Plant Life (Edited by R.C. Worrest and M.M. Caldwell), pp.49-62. Springer-Verlag, Berlin.

32. Green, A.E.S., T. Sawada and E.P. Shettle (1974) The middle ultraviolet reaching the ground', Photochem. Photobiol. 19, 251-259.

33. Green, A.E.S., K.R. Cross and L.A. Smith (1980) Improved analytic characterization of ultraviolet skylight, Photochem. Photobiol. 31, 59-65.

34. Schippnick, P.F. and A.E.S. Green (1982) Analytical characterization of spectral actinic flux and spectral irradiance in the middle ultraviolet, Photochem. Photobiol. 35, 89-101.

35. Braslau, N. and J.V. Davé (1973) Effects of aerosols on the transfer of solar energy through realistic model atmospheres, J. Appl. Meteorol. 12, 601-615.

36. Braslau, N. and J.V. Davé (1973) Effect of aerosols on the transfer of solar energy through realistic model atmospheres. Part II: partly-absorbing aerosols, J. Appl. Meteorol. 12, 616-619.

37. Braslau, N. and J.V. Davé (1973) Effect of aerosols on the transfer of solar energy through realistic model atmospheres, part III: ground level fluxes in the biologically active bands 0.3850-0.3700 microns, IBM research report, RC 4308.

38. Davé, J.V. and P. Halpern (1976) Effects of changes in the ozone amount on the ultraviolet radiation received at sea level of a model atmosphere, Atmos. Environ. 10, 547-555.

39. J.J. Michalsky (1988) *The Astronomical Almanac's* algorithm for approximate solar position (1950-2050), Sol. Energy. 40, 227-235.

40. Parisi, A.V. and N. Downs (2004) Cloud cover and horizontal plane eye damaging solar UV exposures, Int. J. Biometeorol. 49, 130-136.

41. World Health Organization, World Meteorological Organization, United Nations Environment Programme & International Commission on Non-Ionizing Radiation Protection (2022) Global solar UV index: a practical guide, World Health Organization WHO/SDE/OEH/02.2. Available at: https://apps.who.int/iris/handle/10665/42459. Accessed on 12 July 2022.

42. Diffey, B.L., C.T. Jansén, F. Urbach and H.C. Wulf (1997) The standard erythema dose: a new photobiological concept, Photodermatol. Photoimmunol. Photomed. 13, 64-66.

43. Grant, R.H., G.M. Heisler and W. Gao (1996) Photosynthetically-active radiation: sky radiance distributions under clear and overcast conditions, Ag. For. Meteorol. 82, 267-292.

44. Turnbull, D.J. and A.V. Parisi (2004) Annual variation of the angular distribution of the UV beneath public shade structures, J Photochem. Photobiol. B: Biol. 76, 41-47.

45. Downs, N.J., H.J. Butler, L. Baldwin, A.V. Parisi, A. Amar, J. Vanos and S. Harrison (2019) A site-specific standard for comparing dynamic solar ultraviolet protection characteristics of established tree canopies, MethodsX, 6, 1683-1693.

46. Anderson, C., K. Jackson, S. Egger, K. Chapman and V. Rock (2014) Shade in urban playgrounds in Sydney and inequities in availability for those living in lower socioeconomic areas, Aus. N. Z. J. Public Health, 38, 49-53.

47. Gage, R., C. O'Toole, A. Robinson, A. Reeder, L. Signal and C. Mackay (2017) Wellington playgrounds uncovered: an examination of solar ultraviolet radiation and shade protection in New Zealand, Photochem. Photobiol. 94 (2017) 357-361.

48. Cimino, A., J.E. McWhirter and A. Papadopoulos (2022) An evaluation of the amount, type and use of shade at public playgrounds in Guelph, Ontario, Canada, Health Promot. Chron. Disease Prev. Can. Policy Practice. 42, 209-217.

49. Rzotkiewicz, A., A.L., Pearson, B.V. Dougherty, A. Shortridge and N. Wilson (2018) Systematic review of the use of Google Street View in health research: major themes, strengths, weaknesses and possibilities for future research, Health Place. 52, 240-246.

50. Potente, S., C. Anderson and M. Karim (2011) Environmental sun protection and supportive policies and practices: an audit of outdoor recreational settings in NSW coastal towns, Health Promot. J. Aus. 22, 97-101.

51. Cox, V. and B. Brown (n.d.) Shade audit information guide + tool: a guide for creating shady outdoor spaces, Waterloo Region Shade Work Group, Available at:

https://www.regionofwaterloo.ca/en/health-and-wellness/resources/Documents/ShadeAudit_GuideTool.pdf. Accessed on 15 July 2022.

52. Pal, M. (2005) Random forest classifier for remote sensing classification, International J. Remote Sens. 26, 217-222.

53. Azar, A.T., H.I. Elshazly, A.E. Hassanien and A.M. Elkorany (2014) A random forest classifier for lymph diseases. Comput. Meth. Prog. Bio. 113, 465-473.

54. Belgiu, M. and L. Drăguţ (2016) Random forest in remote sensing: A review of applications and future directions, ISPRS J. Photogram. Rem. Sens. 114, 24-31.

55. Calbó, J., D. Pagès and J-A. González (2005) Empirical studies of cloud effects on UV radiation: a review, Rev. Geophys. 43, Available at: https://doi.org/10.1029/2004RG000155. Accessed 2 October 2022.

56. Josefsson, W. and T. Landelius (2000) Effects of clouds on UV irradiance: As estimated from cloud amount, cloud type, precipitation, global radiation and sunshine duration, J. Geophys. Res. 105, 4927-4935.

57. Josefsson, W. (1986) Solar ultraviolet radiation in Sweeden, Technical Report RMK-53, ISSN 0347-2116, Swedish Meteorological and Hydrological Institute, Norrköping, Sweeden.

58. Na, H.R., G. Heisler, D.J. Nowak and R.H. Grant (2014) Modeling of urban trees' effects on reducing human exposure to UV radiation in Seoul, Korea, Urban For. Urban Gree. 13, 785-792.

FIGURE CAPTIONS

Figure 1. (a) Paradise Park (27.61ºS, 151.94ºE), Google Maps Imagery © CNES/Airbus, Maxar Technologies, Map data (c) 2021 (north at top of image). (b) Paradise Park Shade model including [a] *J. mimosifolia*, [b] *A. cunninghamii*, [c] *P. acerifolia*, [d] low shrubs, [e] unidentified overhanging trees, [f] hexagonal shade structure, [g] park playground, and [h] neighboring residential complex (*y*-axis runs north-south, *x*-axis runs east west).

Figure 2. The Paradise Park shade structure photographed from its southern side and looking north (Image taken 20 July 2021 4:10 pm).

Figure 3. (a) *Platanus acerifolia* photographed in Paradise Park on 20 July 2021 (i - winter) and 16 November 2021 (ii - spring). (b) Summertime circular shade disc model shown in side (i) and plan view (ii) is used to represent the foliage density of all broom-canopy trees located inside the park.

Figure 4. Tree shade projections at 27.61°S, 151.94°Emodeled for the deciduous species *P. acerifolia* onto a horizontal parkland surface at 8:00 am local time (a) 04 January (summer), (b) 17 March (autumn), (c) 13 July (winter), and 20 September (spring). North is at the top of each respective subfigure. The height of the modeled tree is 8 m. Shade discs are located at 2 m, 4 m and 6 m.

Figure 5. (a) *Araucaria cunninghamii* photographed at Paradise Park on 20 July 2021. (b) The shade disc model used to represent the foliage density of evergreen trees located inside Paradise park is shown in side (i) and plan view (ii).

Figure 6. Solid surface vertices of a single shade structure roof panel and central axis tree trunk positions were referenced as Cartesian X and Y coordinates measured with respect to a relative park origin (blue dot). (a) Red dots – three vertices are used to fill a single roof panel of the hexagonal shade structure. (b) Yellow dot – the central axis position of a park tree. (Google Maps Imagery © CNES/Airbus, Maxar Technologies, Map data © 2021).

Figure 7. A generalized basic network architecture of binary Random Forest Classifier decision trees as applied by Fiji WEKA (28) for all image input pixels, x and classified parkland surface objects, k_i. In this case, classified surface objects were individual tree canopies.

Figure 8. Classification result based on the trained Random Forest Classifier model of the Paradise Park image of Figure 1a. Using the Fiji WEKA [28] training algorithm, white pixels were identified as belonging to a parkland tree species and darkly classified pixels were defined as image background.

Figure 9. Boundaries around the circular tree canopies were developed for measuring individual tree canopy diameter and determining the local Cartesian coordinates of tree trunks.

Figure 10. Numbered image regions defined by the Random Forest Classifier algorithm as trees with boundaries for calculation of tree canopy diameter and image coordinates (*x, y*) expressed with respect to the top-upper left of the image (green dot). Local image coordinates of each tree were later expressed relative to the park map origin (blue dot) and expressed in metres (X, Y).

Figure 11. Erythema UV irradiance measured on cloud-free days at the University of Southern Queensland (Paradise Park) using the Bentham DTM300 (solid line) compared to respective semi-empirical erythema UV irradiance calculations (Rundel (31), dashed line). Comparisons are for (a) 04 January 2014 - summer, (b) 17 March 2014 - autumn, (c) 20 September 2013 - spring, and (d) 13 July 2013 - winter.

Figure 12. Example calculation of local site obstructed sky fraction, *OS* of 0.3 (70% sky view) for the centrally located grid square metre park site, *p(x,y)* where *p(x-1,y-1)* is protected by a

tree (green) and the square metre sites *p(x,y+1)* and *p(x+1,y+1)* are protected by a shade structure (magenta).

Figure 13. (a) Park shade pattern photographed on 20 July 2021 at 4:10 pm, and (b) oblique shade projection of the Paradise Park shade structure and nearby trees onto the same outlined playground surface modeled for the period 4:00 to 4:10 pm.

Figure 14. (a) Elevated parkland shade pattern photographed by drone at 9:50 am 16 November 2021. (b) Modeled shade surface pattern derived using parkland surface objects between 9:40 and 9:50 am 16 November 2021.

Figure 15. Paradise Park, summer (04 January 2014) 5:00 am to 7:00 pm (a) shade density, (b) surface ultraviolet exposure (including parkland objects), and (c) surface ultraviolet exposure (excluding parkland objects).

Figure 16. Paradise Park, autumn (17 March 2013) 5:00 am to 7:00 pm (a) shade pattern, (b) surface ultraviolet exposure (including parkland objects), and (c) surface ultraviolet exposure (excluding parkland objects).

Figure 17. Paradise Park, winter (13 July 2013) 5:00 am to 7:00 pm (a) shade density, (b) surface ultraviolet exposure (including parkland objects), and (c) surface ultraviolet exposure (excluding parkland objects).

Figure 18. Paradise Park, spring (20 September 2013) 5:00 am to 7:00 pm (a) shade density, (b) surface ultraviolet exposure (including parkland objects), and (c) surface ultraviolet exposure (excluding parkland objects).

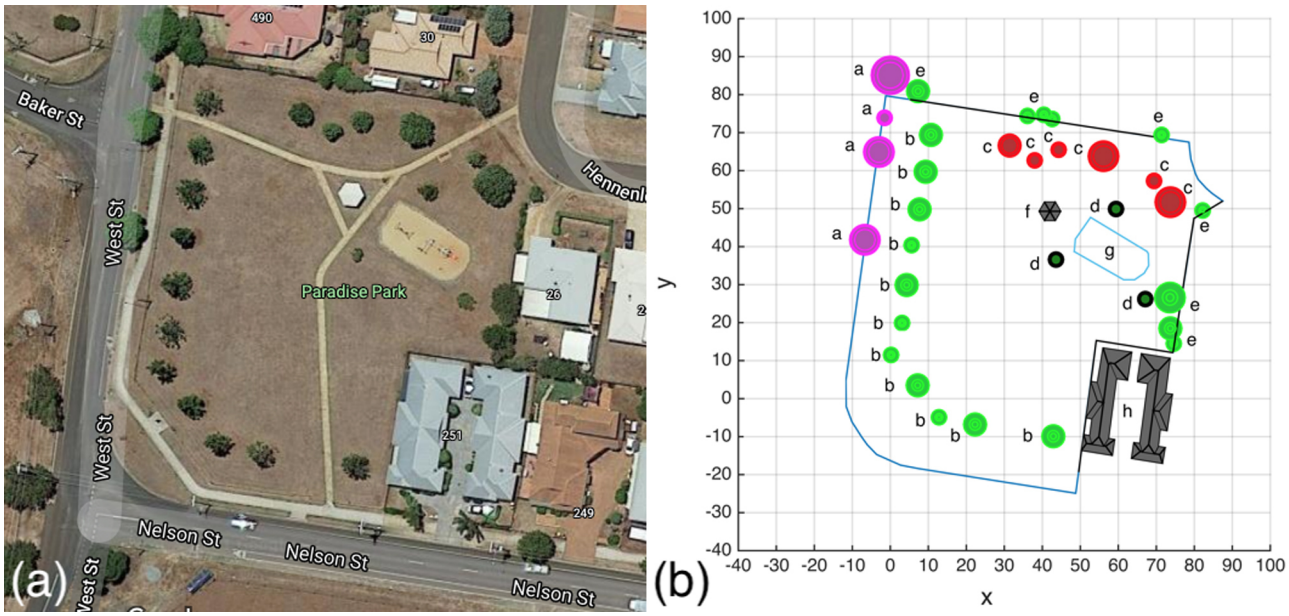

PHP_13745_Figure1.jpg

PHP_13745_Figure2.jpg

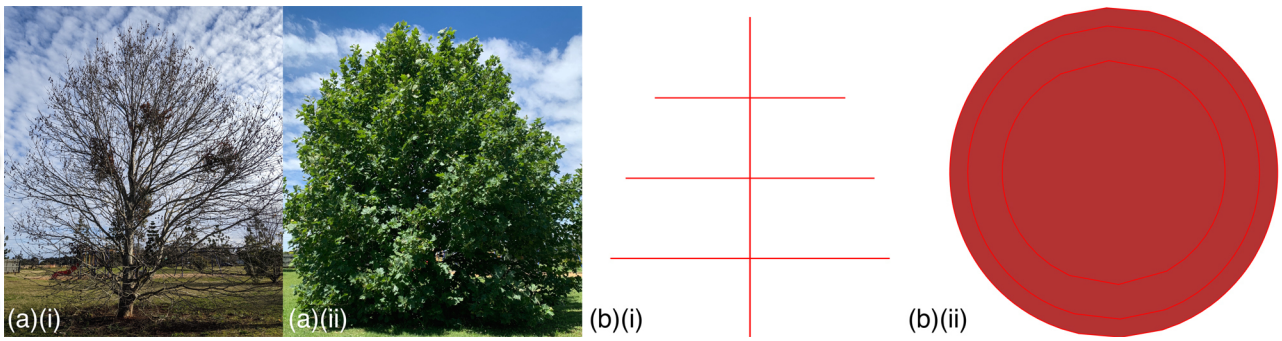

PHP_13745_Figure3.jpg

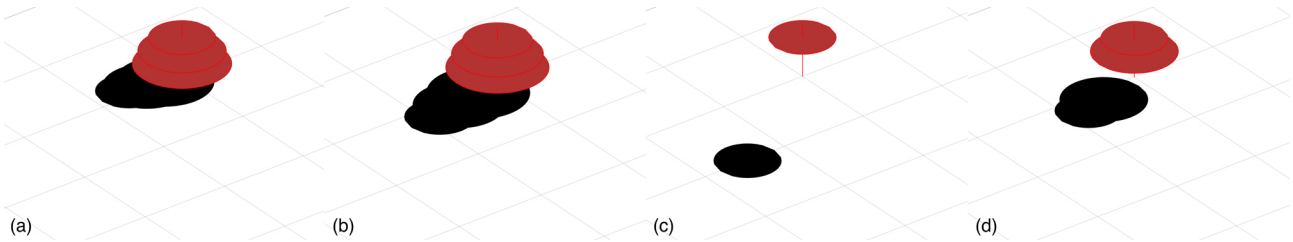

PHP_13745_Figure4.jpg

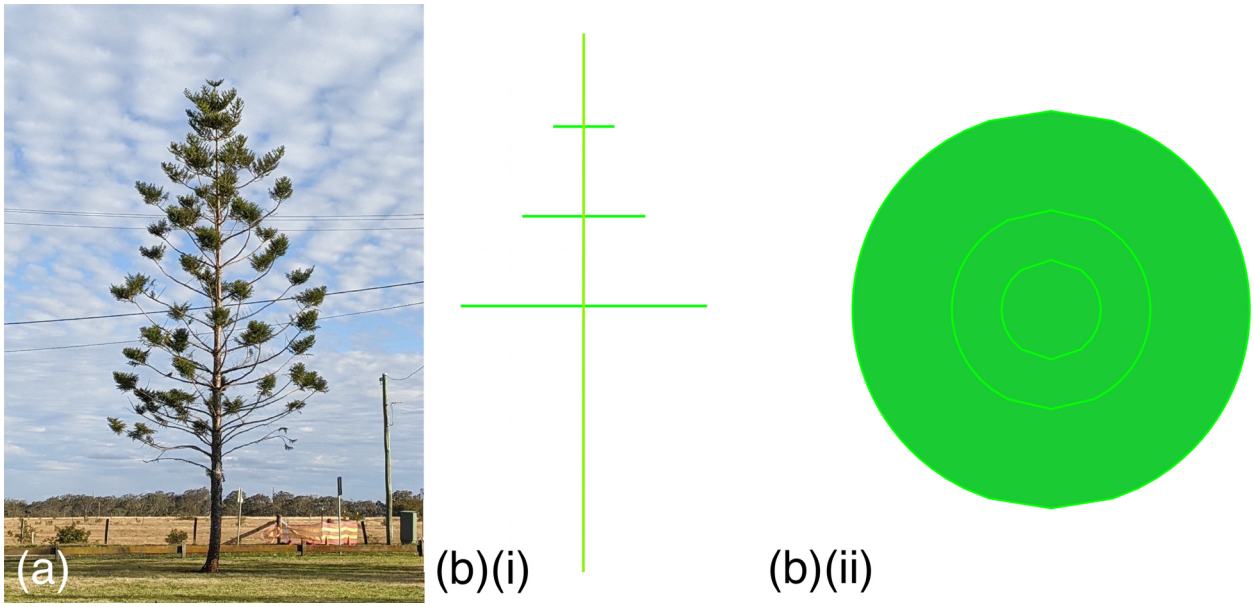

PHP_13745_Figure5.jpg

PHP_13745_Figure6.jpg

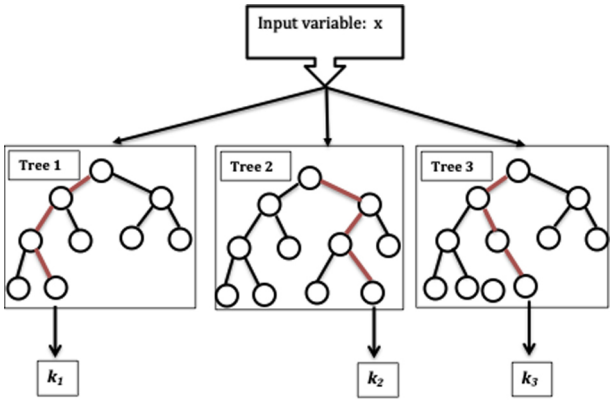

PHP_13745_Figure7.jpg

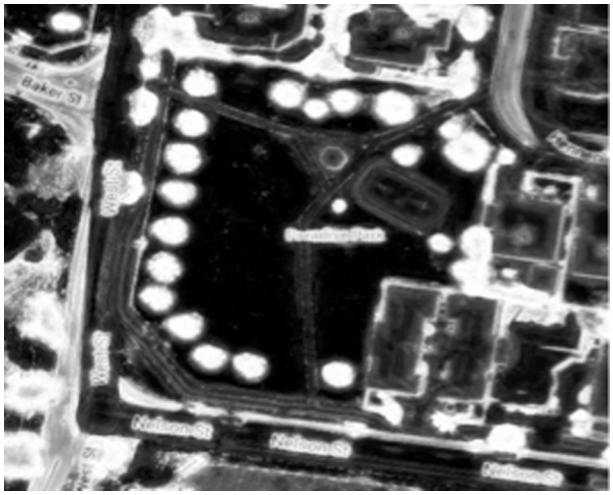

PHP_13745_Figure8.jpg

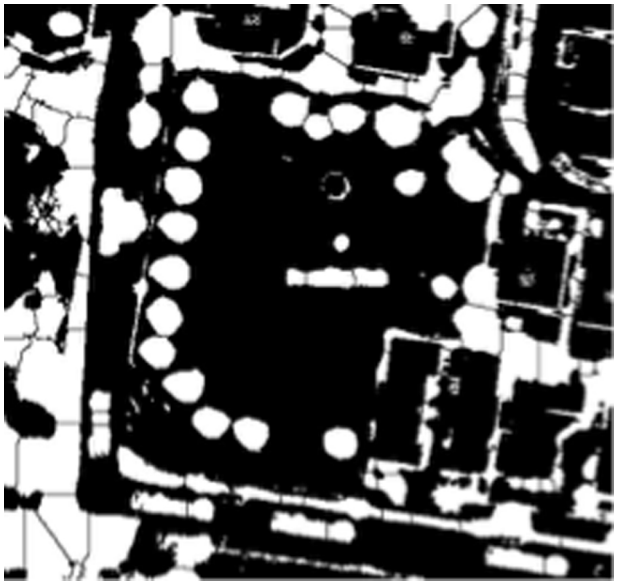

PHP_13745_Figure9.jpg

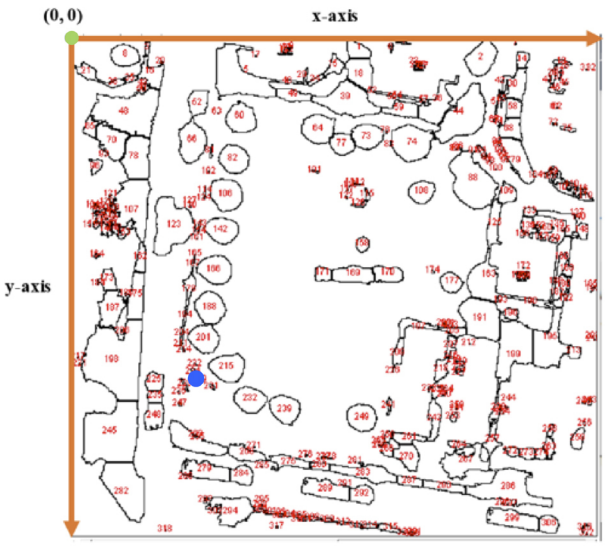

PHP_13745_Figure10.jpg

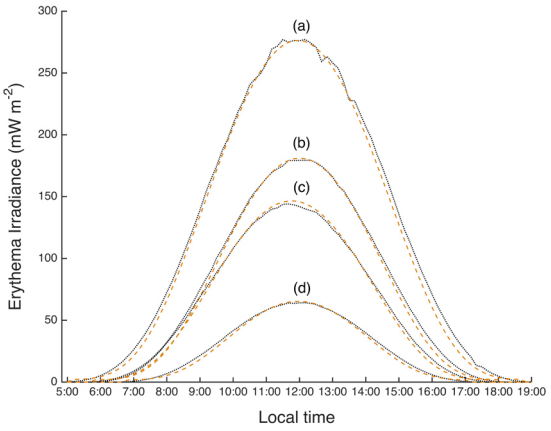

PHP_13745_Figure11.jpg

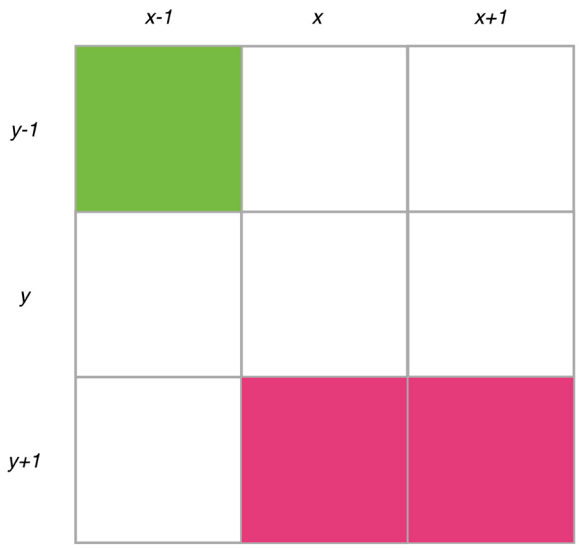

PHP_13745_Figure12.jpg

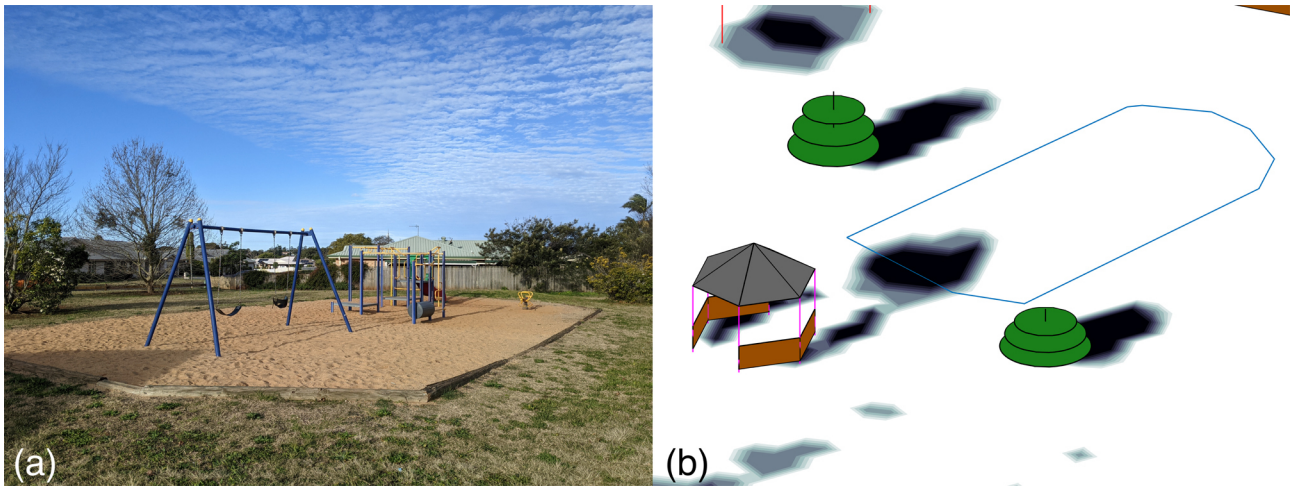

PHP_13745_Figure13.jpg

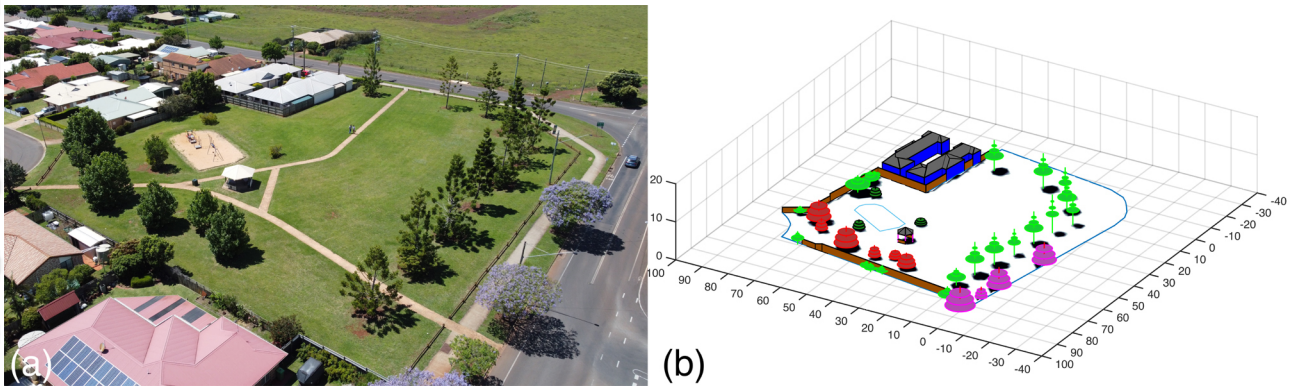

PHP_13745_Figure14.jpg

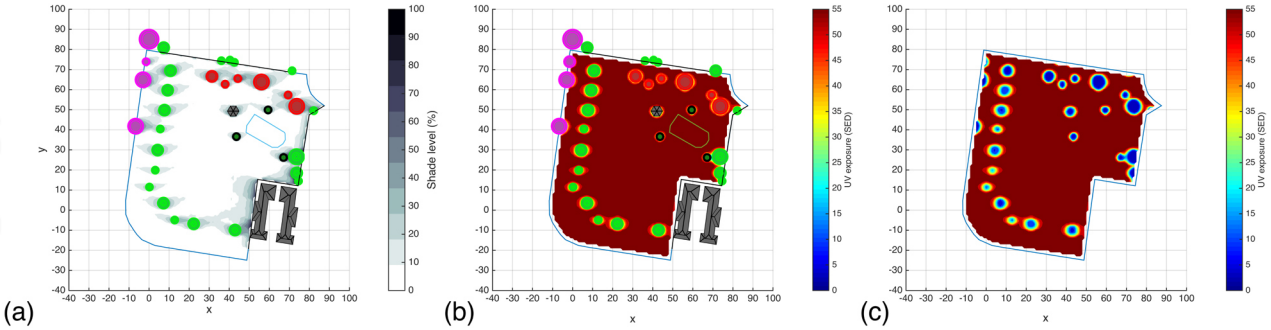

PHP_13745_Figure15.jpg

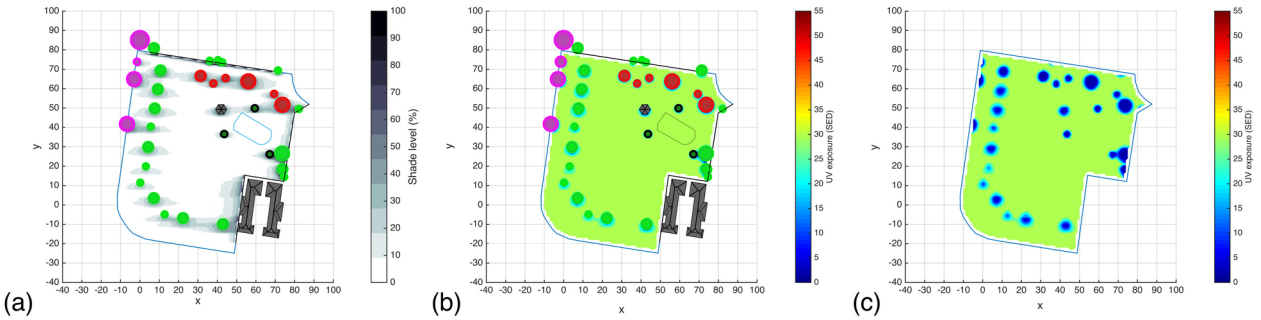

PHP_13745_Figure16.jpg

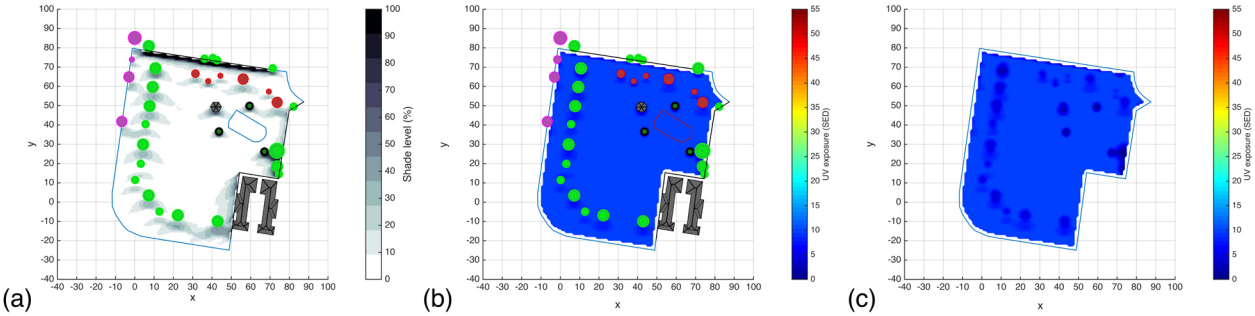

PHP_13745_Figure17.jpg

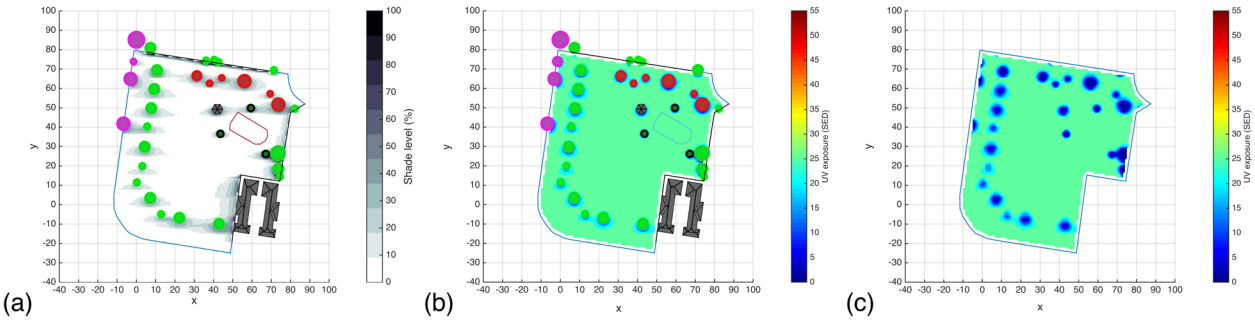

PHP_13745_Figure18.jpg